Computers and Concrete, *Vol. 21, No. 1 (2018) 75-85*
DOI: https://doi.org/10.12989/cac.2018.21.1.075

FE analyses and prediction of bursting forces in post-tensioned anchorage zone

Joung Rae Kim[a] and Hyo-Gyoung Kwak[*]

Department of Civil and Environmental Engineering, Korea Advanced Institute of Science and Technology (KAIST), Daejeon, 305-701, Republic of Korea

(Received May 8, 2017, Revised November 9, 2017, Accepted November 14, 2017)

Abstract. To improve the design equation for the evaluation of the bursting force in the post-tensioned anchorage zone, this paper presents the analyses and design of the post-tensioned (PT) anchorage zone on the basis of three dimensional (3D) finite element (FE) analyses. The structural behavior was investigated through linear elastic finite element analyses upon consideration of the change in design parameters such as the bearing plate size, the eccentricity, and the tendon inclination. Moreover, consideration of the duct hole, which causes an increase of the bursting stress with a change in its distribution along the anchorage zone as well, is emphasized. Since that an exact prediction of the bursting force is the primary interest in design practice, additional parametric analyses are carried out to evaluate the relative contribution of all design parameters in determining the bursting force, and a comparison with the design guidelines mentioned in AASHTO-LRFD has been provided. Finally, an improved design guideline that takes into account the influence by the duct hole is suggested.

Keywords: anchorage zone; bursting force; duct hole; local zone; design guideline

1. Introduction

In post-tensioned prestressed concrete (PSC) beams with mechanical anchorages, the prestressing force is introduced at the end face as a high load concentration, often acting over a small bearing area. At some distance away from the point of load application, the stresses will be uniform and uniaxial, and in these regions the assumption that plane sections remain plane is appropriate (He and Liu 2011). Closer to the applied load, however, the distribution of stresses in the member is more complex. The dispersion of the high local stresses under the bearing plate causes transverse tensile stresses, which may crack the concrete. Longitudinal cracks may form in a zone behind the bearing plate (the bursting zone) or on the end face of the member in an area (the spalling zone) (Breen *et al*. 1994).

Accordingly, these tensile stresses have to be determined with some degree of accuracy in order that the concrete, which possesses little tensile strength of its own, can be adequately reinforced to resist them (Fenwick and Lee 1986). Prior to cracking, the flow of stresses in the bursting zone can be analyzed with the aid of an elastic analysis, which can be effectively used in predicting where and when the first significant cracking of the concrete will occur. After cracking, however, a significant decrease of the maximum tensile stress with the change in its location is accompanied due to the redistribution of the internal stresses (Fenwick and Lee 1986). Nevertheless, the results of elastic analyses traditionally have been used to guide the engineer as to where reinforcement is required and what amount will be needed so that the design will meet safety requirements (Adeghe and Collins 1986).

With the understanding of the stress distribution in the anchorage zone, considerable efforts have been dedicated in evaluating the tensile force for the placement of reinforcements (Guyon 1953, Burdet 1990, He and Liu 2011) on the basis of many mechanical concepts such as the theory of elasticity, the finite element (FE) analysis, and the strut-and-tie method as well as experimental approaches. Related comprehensive reviews on previous research can be found elsewhere (Breen *et al*. 1994, Rogowsky and Marti 1996, Songwut 2004, Callaghan and Bayrak 2008, Zhou *el al*. 2015). Moreover, many experimental and numerical studies have allowed the obtained results to be implemented in many design codes (Schlaich *et al*. 1987, Burdet 1990, Wollman 1992, Sanders and Breen 1997). In particular, the design formula mentioned in the AASHTO-LRFD design guidelines (AASHTO-LRFD 2012), which was introduced through extensive finite element analyses by Burdet (1990) to provide guidance for designing the anchorage zone, is popularly used in the design practice. As shown in Eq. (1), the design formula mentioned in the AASHTO-LRFD design guideline is composed of two parts for the evaluation of the bursting force. The first part, originally proposed by Mörsch (1924), takes into account the influence by the size of bearing plate and the other part implements the contribution by the inclination of the anchorage device.

$$T_{burst} = 0.25\Sigma P\left(1-\frac{a}{h}\right) + 0.5|\Sigma(P(\sin\alpha)| \qquad (1)$$

where P is the applied anchor load, a is the width of the bearing plate, h is the height of the anchorage block, and

∗Corresponding author, Professor
E-mail: kwakhg@kaist.ac.kr
[a]Ph.D. Student

ISSN: 1598-8198 (Print), 1598-818X (Online)

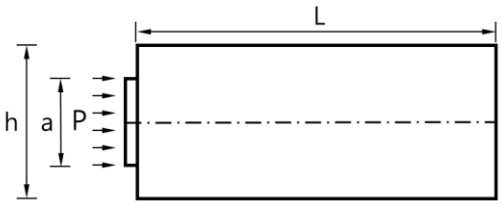

(a) Anchorage zone without duct hole

(b) Anchorage zone with duct hole

Fig. 1 Anchorage zone specimen

α is the inclination of the duct tube.

Since Eq. (1) was suggested basically on the basis of two dimensional (2D) FE analyses and does not have an adequate theoretical basis in considering the design parameters, this equation usually gives conservative results in most cases. To improve this equation, accordingly, He and Liu (2011) suggested an improved formula that can consider the contribution by the eccentricity of tendon, with the use of the compression-dispersion method (Sahoo 2009), and they verified its efficiency through FE analyses. This formula considers all the influencing factors such as the anchorage plate size, the eccentricity, and the tendon inclination and represents the explicit expression.

In spite of various formulas suggested by many researchers (Brenda 2009, He and Liu 2011) and also described in many design codes (CEB-FIP 2010, AASHTO-LRFD 2012), there is no equation that considers the duct hole effect induced from the presence of the sheath tube in the concrete matrix. As is well known from the elastic theory, the hole within the elastic body causes a stress concentration. Shen *et al.* (2014) suggested two-dimensional FEM model with duct hole and it concluded that the influence of duct hole effect is less than 5%. However, the duct hole in two dimensions can't idealize the circular hole which cause the stress concentration around the hole. Moreover, when an infinite plate with a circular hole is subjected to uniform stress on two parallel edges far removed from the hole, then the developed maximum stress will be three times the applied stress. This means that the duct hole may cause not only the stress concentration but also the change in a stress distribution around the hole.

Accordingly, since the placement of reinforcing steel at the anchorage zone is based on the evaluation of the bursting force and the bursting force must not be underestimated, Eq. (1) cannot be directly used in its present form in the design of an anchorage zone without in-depth analyses to verify its accuracy and to bring the necessary adjustments. Upon this background, many parametric studies to evaluate the relative contribution of all design parameters in determining the bursting force have been conducted in this paper on the basis of 3D FE analyses

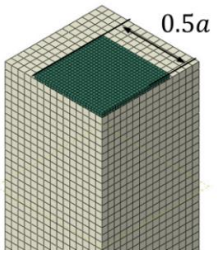

(a) without anchorage device and duct hole

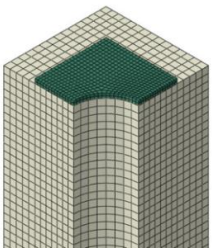

(b) with duct hole only

Fig. 2 Anchorage block with square bearing plate

with ABAQUS, and then an improved formula to evaluate the bursting force in the post-tensioned anchorage zones is suggested.

2. FE idealization and verification

Since the numerical analyses conducted in this paper are based on a linear elastic analysis, the stress-strain relations of concrete and steel do not need to be defined. Only the modulus of elasticity and Poisson's ratio for concrete and steel are required. The elastic modulus of concrete and steel is defined according to the formulas $E_c = 8{,}500\sqrt[3]{f_c'} = 28{,}000$ MPa and $E_s = 210$ GPa defined in the KCI design code (2009) that is equivalent to the ACI design code (2014), respectively, and the Poisson's ratios for concrete and steel have values of $\nu_c = 0.18$ and $\nu_s = 0.33$.

As shown in Fig. 1, two different anchorage blocks of (1) the anchorage block without anchorage device and duct hole (see Fig. 1(a)) and (2) the anchorage block with duct hole (see Fig. 1(b)) are considered for finite element analysis. The specimens are composed of two parts of the concrete matrix and the bearing plate. The concrete matrix has square section with the width of h and the rectangular bearing plate has the width of a. As the specimen is assembled, the constituent two parts of the anchorage zone must be in constant contact with each other. Namely, a perfect bond is applied in the numerical modeling of the specimens. The loading process is guaranteed through displacement control of the bearing plate. Since the bearing plate is sufficiently rigid, the application of compressive force through the limited area of anchor head does not give any meaningful difference in the numerical results.

In this paper, 20-node 3D solid elements (named C3D20 in ABAQUS) are adopted to consider the geometric effect of the bearing plate and three-dimensional solid elements (named C3D10R element in ABAQUS) are used in the numerical modeling of the concrete matrix of the anchorage zone, respectively (see Fig. 2). Moreover, to ensure consistency in numerical modeling, the mesh size of each finite element is based on equal length of 17 mm regardless of the difference in the size of concrete block. The dimensions of 17 mm×17 mm×17 mm determined through the convergence test of the FE mesh size are based in modeling the concrete matrix, and the element mesh size for the bearing plate is based on equal length of 8.5 mm regardless of the difference in the size of specimens because

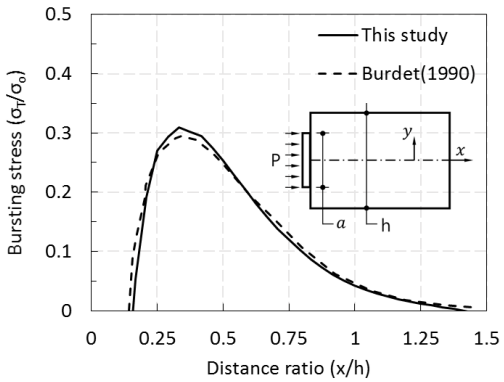

Fig. 3 Comparison of bursting stress in an anchorage block

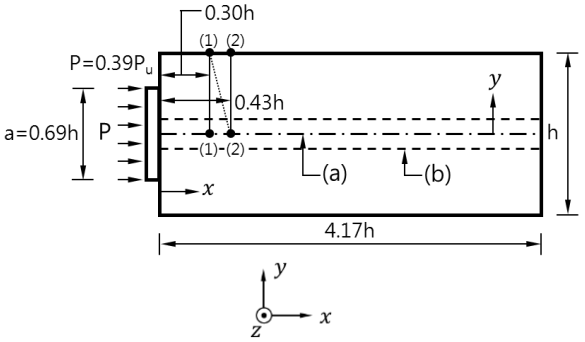

Fig. 4 Section view of the model in Fig. 2(a)

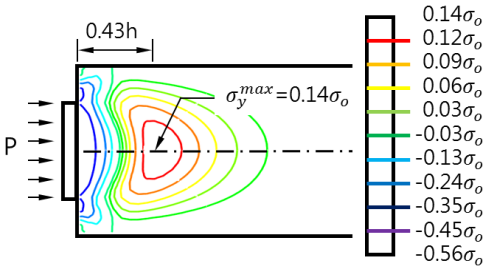

(a) Radial direction (y axis)

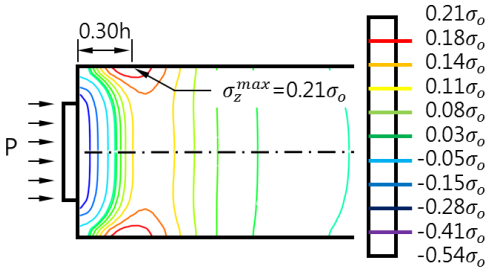

(b) Tangential direction (z axis)

Fig. 5 Bursting stress contour developed in the model in Fig. 4

of the thickness of the bearing plate. Because of the structural symmetry, in advance, only a quarter portion of the specimen is represented in numerical modeling by ABAQUS.

To verify the reliability of the constructed FE model, the numerical results were compared to those obtained by Burdet (1990), because Burdet's numerical results obtained from the linear elastic stress analyses were based on the construction of Eq. (1). Fig. 3 shows a typical example for the comparison of the bursting stress (σ_T) along the length (x-direction in Fig. 3) between the Burdet's results and the numerical results obtained by the FE idealization used in Fig. 2. The ratio of the bearing plate size (a) to the concrete block width (h) was assumed to be 0.3 and σ_0 in Fig. 3 means the uniform average normal stress developed by the application of a concentrated load to the anchorage head. As shown in Fig. 3, the bursting stress distributions obtained by the constructed FE idealization of the anchorage block is almost the same as that obtained by Burdet, even though the maximum bursting stress shows a slight difference of $0.014\sigma_o$, which is still negligibly small. This means that the slightly modified FE idealization can effectively be used in the linear elastic analyses of anchorage blocks.

3. Numerical analyses of anchorage block

3.1 Influence of bearing plate size

The prestressing force in a post-tensioned (PT) concrete member is transferred from tendon to concrete essentially by direct bearing through the anchorage. In the immediate vicinity of the bearing area, very high compressive stresses exist and transverse tensile stresses develop in the nearby concrete (Kim *et al.* 2014). The high compressive stresses immediately behind the bearing plate can cause bursting of concrete, which generates high tensile stresses in the transverse direction away from the plate. The tensile stress field is such that splitting cracks tend to appear in the horizontal plane accompanied by spalling cracks at the corners of the member. Fig. 5 presents a typical example of the distribution of the transverse stresses along the central axis. Accordingly, to resist these tensile stresses, additional reinforcement is provided within the region where the tensile stresses are developed, and the amount is determined on the basis of an exact evaluation of the bursting force.

It is well known that the distribution of the transverse stresses is very largely dependent upon the ratio of the bearing plate width (a) to the height of the anchorage block (h), and the relationship to evaluate the bursting force has been proposed (Mörsch 1924, Brenda 2009, He and Liu 2011). Among these relations, a simple expression in Eq. (2) suggested by Mörsch (1924) is popularly used and also adopted in the AASHTO-LRFD design guideline for the evaluation of the bursting force T_{burst} obtained by integrating the bursting stresses in a concentric anchorage block.

$$T_{burst} = 0.25P\left(1 - \frac{a}{h}\right) \quad (2)$$

where P is the applied anchor load.

To verify the reliability of Eq. (2), parametric studies were conducted with the change in the bearing plate width in the finite element model. Fig. 4 shows the section view of a test specimen with h=360 mm and a=0.69 h=250 mm. Since three dimensional FE analyses were carried out, two transverse stresses across the central axis (the radial bursting stress σ_y and the tangential bursting stress σ_z)

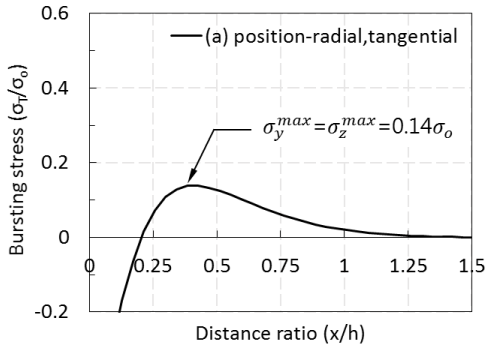

Fig. 6 Bursting stress distribution along (a) position in Fig. 4

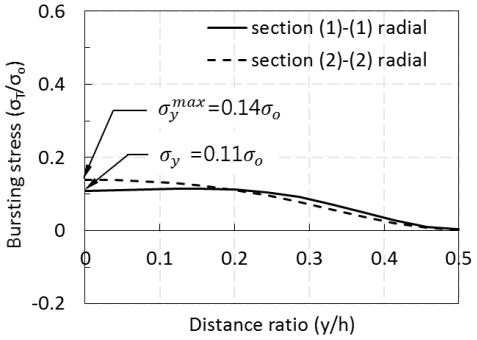

(a) Radial bursting stress distribution

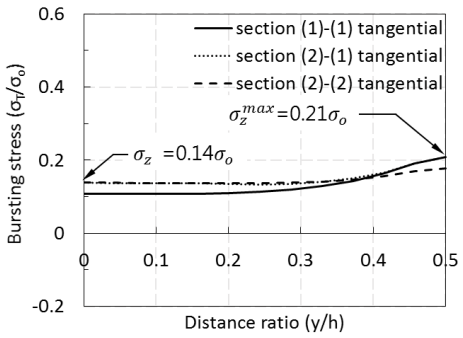

(b) Tangential bursting stress distribution

Fig. 7 Transverse stress distribution across the depth

were evaluated. Figs. 5 and 6 represent the stress contour lines and the stress distributions along the central axis for the corresponding bursting stresses, respectively, where $\sigma_o = P/h^2$ denotes the uniformly distributed basic stress. As shown in Fig. 5, the tangential bursting stress shows the maximum value on the outer surface but a uniform distribution across the depth, in contrast with the radial bursting stress (σ_y), which has the maximum value at the very interior center point. As expected, on the other hand, Fig. 6 shows that both stresses have the same values along the central axis because of the symmetric condition.

This difference in the stress distribution can be explained through the distribution of the transverse stresses across the depth, as shown in Fig. 7. Differently from the radial bursting stress σ_y, the tangential bursting stress σ_z maintains almost a constant value across the depth. From the obtained stress distributions, it can be inferred that the bursting force needs to be evaluated on the basis of the tangential bursting stress, which was usually not considered, rather than on the basis of the radial bursting stress because the use of the tangential bursting stress produces a larger bursting force. The bursting force T_{burst} in Eq. (2) was also derived from a two dimensional analysis of the anchorage block with a unit thickness (Mörsch 1924, Burdet 1990) on the basis of the assumption that the bursting stress maintains a constant value across the width (z-direction in Fig. 4). In the case of the example specimen in Fig. 4, the bursting force evaluated from the three dimensional finite element analysis was T_{anal}=0.069P and that obtained by Eq. (2) was T_{burst}=0.076P. Both bursting forces basically present similar values, although Eq. (2) gives a slightly conservative result.

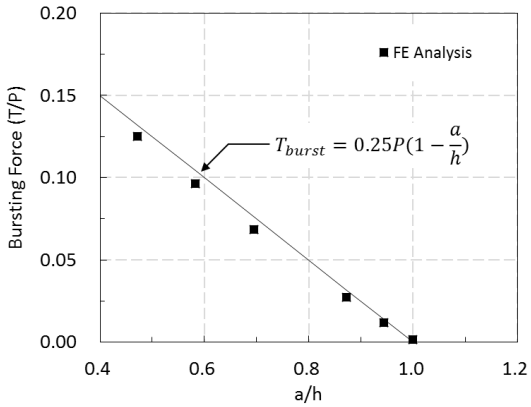

Fig. 8 Comparison of analysis results with Eq. (2)

With the change in the anchorage plate width, the three dimensional FE analyses were conducted and the obtained results can be found in Fig. 8. As shown in this figure, the finite element analysis results correspond very closely to the results by Eq. (2) in which the value of 0.25 was originally suggested by Mörsch (1924). This comparison of the obtained results indirectly shows the reliability of the finite element idealization of anchorage blocks and the accuracy of the obtained results.

3.2 Influence of duct hole

Since the anchorage block, which is provided to anchor the prestressing tendons in a PT concrete member, contains a duct hole along the length, the influence of the duct hole needs to be considered. To investigate the duct hole effect, Burdet (1990) performed a 3D finite element analysis for an anchorage block with a duct hole, and the obtained results were compared with those by a 2D finite element analysis for an anchorage block without considering a duct hole. Since the difference in the bursting stress distribution between both results was relatively small, Burdet (1990) reported that the influence of the duct hole may be ignored.

When the size of the duct hole is relatively small, its influence can be ignored as was assumed by previous researchers (Guyon 1953, Saadoun 1980, Burdet 1990) but an increase in the size of the duct hole requires an additional consideration in determining the bursting force because the duct hole causes an increase of the bursting stresses by the stress concentration around the hole. On the

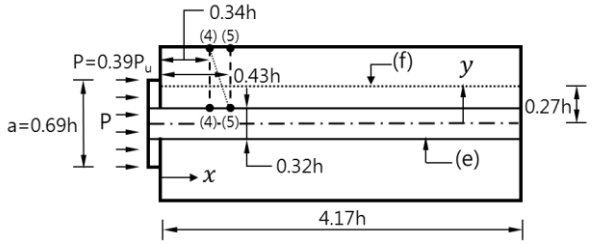

Fig. 9 Section view of the model in Fig. 2(b)

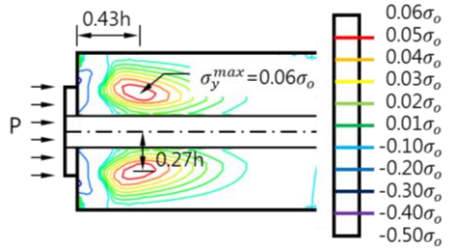

(a) Radial direction (y axis)

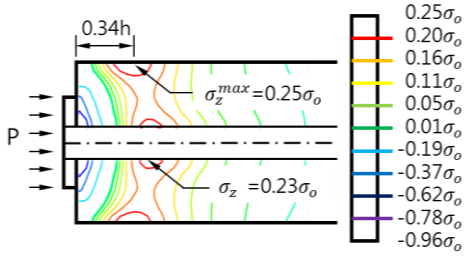

(b) Tangential direction (z axis)

Fig. 10 Bursting stress contour developed in the model in Fig. 9

basis of experimental results, Douglas and Trahair (1960) noted that the presence of the central duct hole affects the stress distribution in the anchorage zone sufficiently to produce a significant decrease in the ultimate load due to an increase of the bursting stress and force.

Accordingly, to discuss the change in the bursting force according to the consideration of the duct hole, three dimensional finite element analyses were conducted. The numerical analyses with the specimen in Fig. 1(b) were performed, and the reference plans to determine the bursting stresses and force are described in Fig. 9 in which the diameter of the duct hole b was assumed to be b=0.32 h=114 mm, and sections (e) and (f) correspond to the duct hole surface and the point that produces the maximum radial bursting stress σ_y, respectively (see Fig. 10).

Figs. 10 and 11 represent the stress contour lines and the stress distributions along the length direction for the corresponding bursting stresses. As shown in Fig. 10, the maximum radial bursting stress σ_y does not occur along the outer surface of the duct hole and its magnitude is also negligibly small. However, the tangential bursting stress σ_z shows the maximum value at the surface of the duct hole and its magnitude is $\sigma_z = 0.23\sigma_o$, which is about 64% larger than the maximum bursting stress obtained at the anchorage block without the duct hole (see Fig. 9). This means that the existence of the duct hole causes a shift in the bursting stress distribution with an increase of the

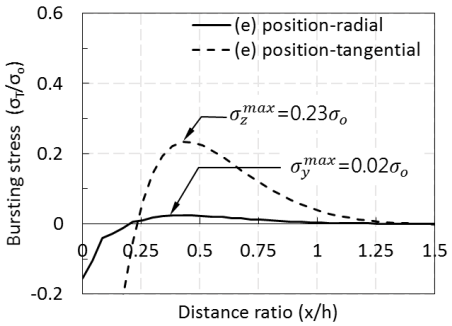

(a) Stress distribution along (e) position

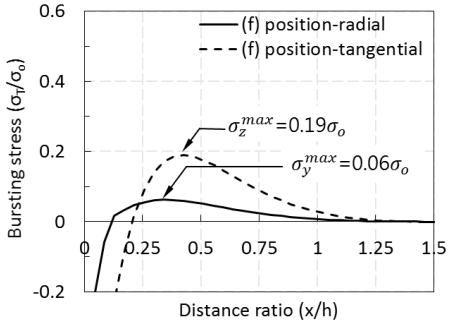

(b) Stress distribution along (f) position

Fig. 11 Bursting stress distribution along (e) and (f) positions in Fig. 9

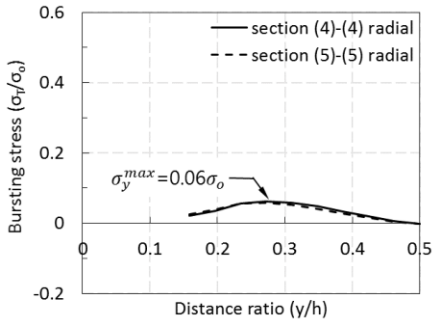

(a) Radial bursting stress distribution

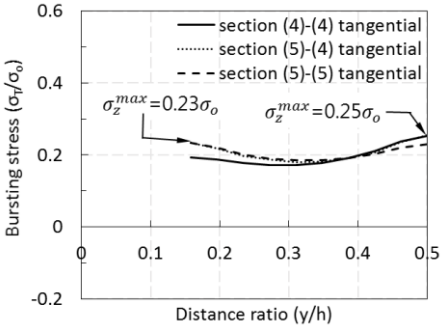

(b) Tangential bursting stress distribution

Fig. 12 Bursting stress distribution across the depth (See Fig. 9)

tangential bursting stress and a decrease of the radial bursting stress. This shift in the stress distribution has been maintained along the entire length of the anchorage block, as shown in Fig. 11. Very similar results for the shift of the bursting stress distribution were also obtained by Douglas and Trahair (1960) from their experimental study. Fig. 12

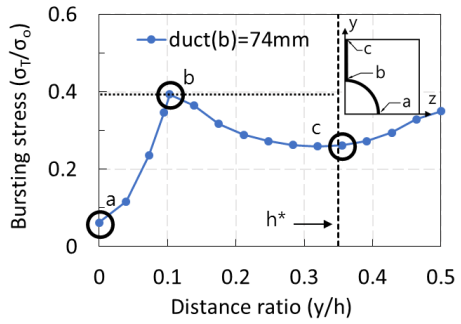

(a) d_{duct}=74 mm

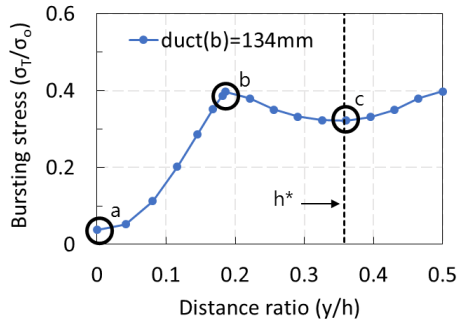

(b) d_{duct}=134 mm

Fig. 13 Tangential bursting stress distribution across the depth in the model in Fig. 2(b)

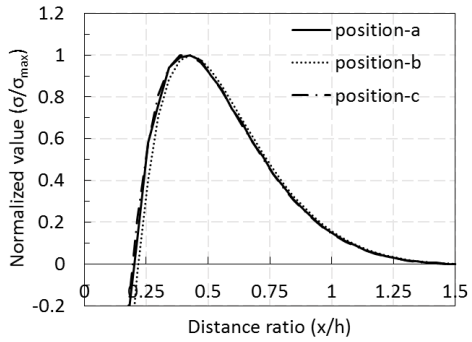

(a) d_{duct}=74 mm

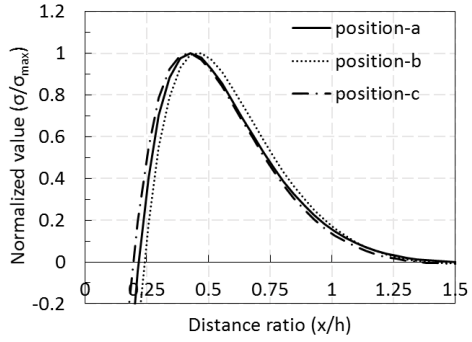

(b) d_{duct}=134 mm

Fig. 14 Tangential bursting stress distribution along the length in the model in Fig. 2(b)

also shows the variation of the bursting stresses across the depth of the anchorage block. As reviewed in Fig.7, the tangential bursting stress σ_z maintains an almost constant value across the depth. Accordingly, the bursting force needs to be evaluated on the basis of the tangential bursting stress even in the case of the anchorage block with a duct hole.

The evaluation of the bursting force will be made by considering the variation of the tangential bursting stresses along the length and across the depth. However, the existence of a duct hole causes complexity in the bursting stress distribution. As shown in Fig. 13, which represents the stress distribution of the tangential bursting stresses, the bursting stress shows a relatively small variation in the regions below and above the duct hole (*b* to *c* region in Fig. 13) but decreases in the region spanning *b* to *a* in Fig. 13. Accordingly, to take into account the stress variation across the depth, the equivalent depth h^* has been evaluated by the relation $h^* = \int \sigma_z dy / \sigma_z^{max}$. The bursting force then can be determined by integrating the bursting stress along the length, $T_{burst} = \int \sigma_z h^* dx$. This integration is possible when the tangential bursting stress represents the same stress distribution along the length, and Fig. 14, which represents a part of the normalized stress distributions along the length for the tangential bursting stresses at points *a*, *b*, and *c* in Fig. 13, shows the soundness of this approximation.

Upon the parametric studies with variation in the size of the duct hole, the evaluated bursting forces are shown in Table 2 and Fig. 15. As shown in this figure, since the existence of the duct hole slightly increases the bursting force together with an increase of the bursting stress, the influence of the duct hole in the anchorage block needs to be considered in the evaluation of the bursting force. However, the relative differences in the bursting force according to the change in the size of duct hole are not as large as expected. This result appears to be induced from characteristic that the maximum tangential bursting stress is not increased in proportion to the size of the duct hole but maintains almost constant values, as shown in Fig. 13, in the case of adopted test specimens with the size of the duct hole ranging from 74 mm (equivalent to 0.21h) to 134 mm (equivalent to 0.37h). However, since the size of the duct hole in real structures is about 0.2h, the test specimens are sufficient to cover the influence of the duct hole in a real structure. Accordingly, the design equation in Eq. (2), which does not take into account the influence of the duct hole, needs to be revised to $T_{burst} = 0.28P\left(1 - \frac{a}{h}\right)$ for an anchorage block with a square bearing plate.

3.3 Influence of eccentricity

The prestressing force is usually applied eccentrically in

Table 1 Bursting force in the anchorage block (*h*=360 mm)

a	*a/h*	T_1/P				
		no duct	*b*=74 mm	*b*=94 mm	*b*=114 mm	*b*=134 mm
170	0.472	0.125	0.141	0.144	0.146	0.141
210	0.583	0.097	0.109	0.111	0.113	0.113
250	0.694	0.069	0.078	0.081	0.083	0.085
314	0.872	0.027	0.033	0.034	0.035	0.037
340	0.944	0.012	0.014	0.015	0.016	0.017
360	1.000	0.002	0.002	0.002	0.002	0.002

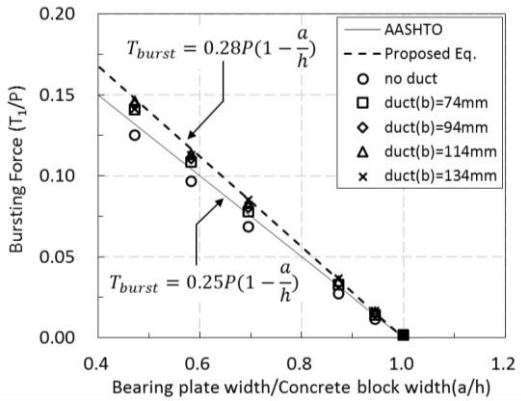

Fig. 15 Bursting force in the anchorage block with a duct hole

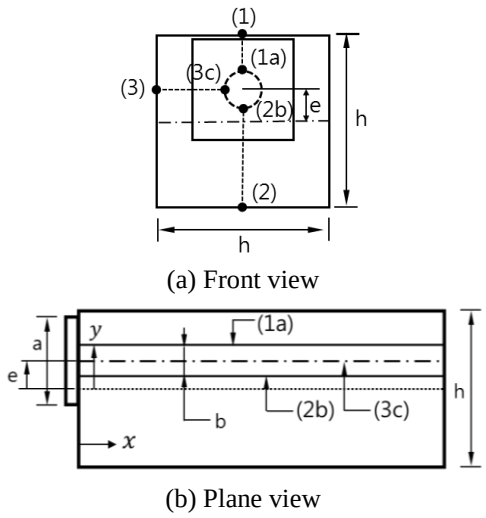

Fig. 16 Description of eccentric anchorage zone

the anchorage zone and develops a non-uniform trapezoidal distribution of the normal stresses across the depth because of the additional application of the bending moment caused by the eccentricity. In advance, the eccentrically loaded prestressing force also causes a change in the bursting stress distribution with an increase of the maximum bursting stress. Previous studies (Yettram and Robbins 1970, Burdet 1990) proved that the bursting force in an eccentric anchorage zone could be determined by using Guyon's symmetrical prism approach and this approach was adopted in the CEB-FIP design code (2010). However, since the eccentricity basically decreases the bursting force to be resisted in the anchorage block (Songwut 2004, He and Liu 2011) in spite of an increase of the maximum bursting stress, most design codes exclude the consideration of the eccentricity effect in the evaluation of the bursting force and the AASHTO-LRFD is also not exceptional.

To review the variation of the bursting force with an increase of the eccentricity, three dimensional finite element analyses were conducted. Fig. 16 shows a front view and a plane view of the test specimen, and Table 3 represents the eccentricities considered. Seven different cases were analyzed, and the obtained bursting forces T are summarized in Table 3, where P and T_o denote the applied

Table 2 Comparison of the bursting force according to the eccentricity

a (mm)	b (mm)	e (mm)	e/h	T/P	T_o/P	T/T_o
170	74	10	0.028	0.141	0.141	1.000
170	74	20	0.056	0.139	0.141	0.986
170	74	40	0.111	0.137	0.141	0.972
170	74	60	0.167	0.136	0.141	0.965
170	74	95	0.264	0.133	0.141	0.943
250	74	20	0.056	0.074	0.078	0.949
340	74	10	0.028	0.012	0.014	0.857

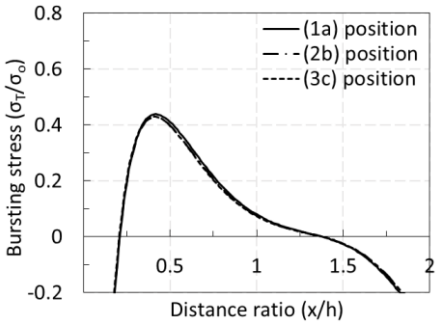

(a) e=10 mm (e=0.028h)

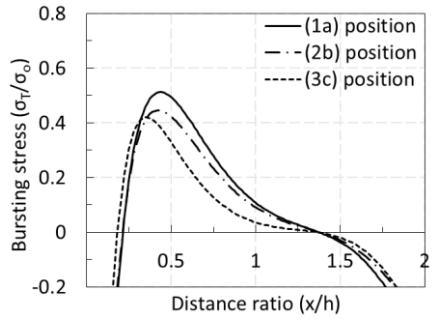

(b) e=40 mm (e=0.111h)

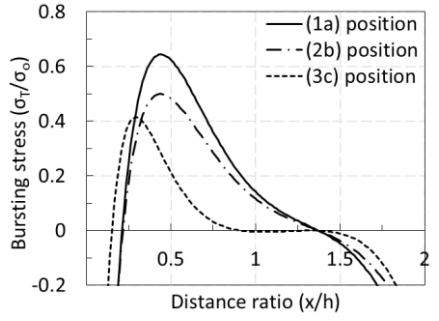

(c) e=60 mm (e=0.167h)

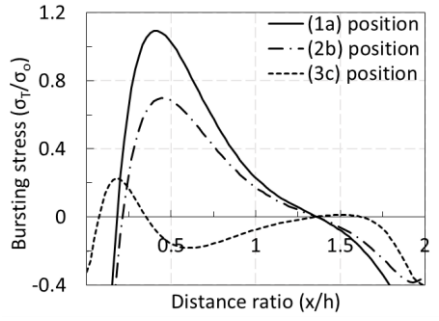

(d) e=95 mm (e=0.264h)

Fig. 17 Bursting stress distribution according to the eccentricity (a=170 mm, h=360 mm)

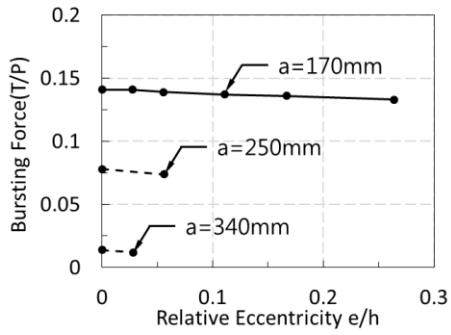

(a) Bursting force

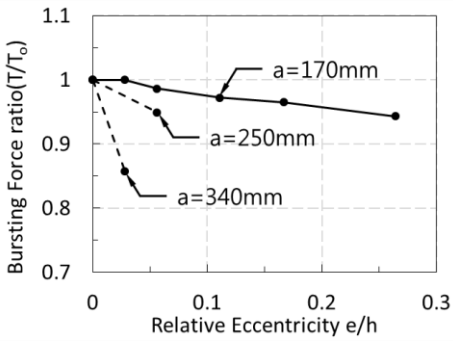

(b) Ratio of bursting force

Fig. 18 Influence of the bearing plate eccentricity on bursting force

prestressing force and the bursting force evaluated when $e = 0$, respectively. As shown in this table, an increase of the eccentricity while maintaining the equal size of the bearing plate causes a decrease of the bursting force, and the same results were also obtained by many previous researchers (Burdet 1990, Songwut 2004, He and Liu 2011).

Fig. 17 shows the distribution of the bursting stresses along the length direction with the change in the eccentricity when the bearing plate height (a) is 170 mm. As shown in this figure, the magnitude of the maximum bursting stress increases with an increase of the eccentricity in the bearing plate, and the maximum stresses were developed along the top face of the duct hole corresponding to point (1a) in Fig. 16(a). However, because of the reduction of the affected region (section (1a)-(1) in Fig. 16(a)) together with a rapid decrease of the bursting stress along the line (2b)-(2) in Fig. 16(a), the resultant bursting force actually decreases.

Fig. 18, which represents the variation of the bursting forces with an increase of the eccentricity, shows that an increase of the eccentricity decreases the bursting force. In advance, the use of a relatively larger size bearing plate develops a smaller bursting force as shown in Table 3, and the reduction ratio of the bursting force according to the eccentricity of the anchorage plate is usually increased (see Fig. 18(b)). Accordingly, upon the obtained analysis results, it can be concluded that the eccentricity of the bearing plate will decrease the bursting force, although the magnitude of this decrease is relatively small, and the influence of the eccentricity may be ignored in design practice. However, as shown in Fig. 17, since an increase of the bursting stress will move up the cracking initiation time in the anchorage zone, additional attention may be required in the serviceability aspect.

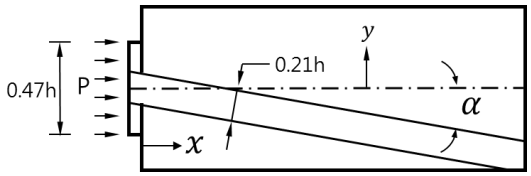

Fig. 19 Geometry of anchorage zone with inclined tendon

3.4 Influence of inclined tendon

Usually post-tensioning tendons have some inclination in the anchorage zone, and this inclination is less than 20 degrees (Burdet 1990, He and Liu 2011). When an inclined load is applied to the anchorage block, the vertical force component of the load will disturb the flow of forces in the anchorage zone while developing an increase of the bursting tensile stress. Breen and Stone's research results (1984) indicate that the decrease of cracking load is about 1% per degree of inclination, and Oh *et al*. (1995) obtained similar results in their experimental study. The influence of an inclined tendon was also analyzed through finite element analyses and the use of the strut-and-tie model (Burdet 1990, He and Liu 2010). Since the inclined prestressing force will increase the bursting stress and the corresponding bursting force to the normal direction of the tendon (Burdet 1990), most design codes require that the influence of inclined tendons be taken into account. The AASHTO-LRFD design guideline also considers the influence of the inclined tendon by

$$T_{burst} = 0.5|\sum Psin(\alpha)| \quad (3)$$

where P is the applied anchor load and α is the inclination angle.

To review the reliability of Eq. (3), parametric studies have been conducted with the change in the inclination angle of the duct hole up to 20 degrees. Since the inclination of the duct hole changes the bursting stress direction to be perpendicular to the tendon axis (Burdet 1990), the bursting force was evaluated by considering the bursting stress direction together with the duct hole. Twenty-four specimens were composed by combining of six different bearing plate sizes (a=170 mm, 210 mm, 250 mm, 314 mm, 340 mm and 360 mm) and four different duct hole sizes (b=74 mm, 94 mm, 114 mm and 134 mm), and Fig. 19 shows a plane view of a typical anchorage block with the inclination angle α. Some a part of the obtained results are shown in Fig. 20, where in which AASHTO represents the results evaluated from Eq. (3), that is, T/P=0.5sinα. 'This study' in Fig. 20 denotes the results determined by subtracting the analysis results when α=0 from the obtained results for the specimen with the inclination angle α.

As shown in Fig. 20, the bursting forces obtained by the finite element analyses increased with an increase of the inclination angle, but the rate of increase is reduced when the inclination angle is larger than 10 degrees. This phenomenon appears to be caused by the change in the

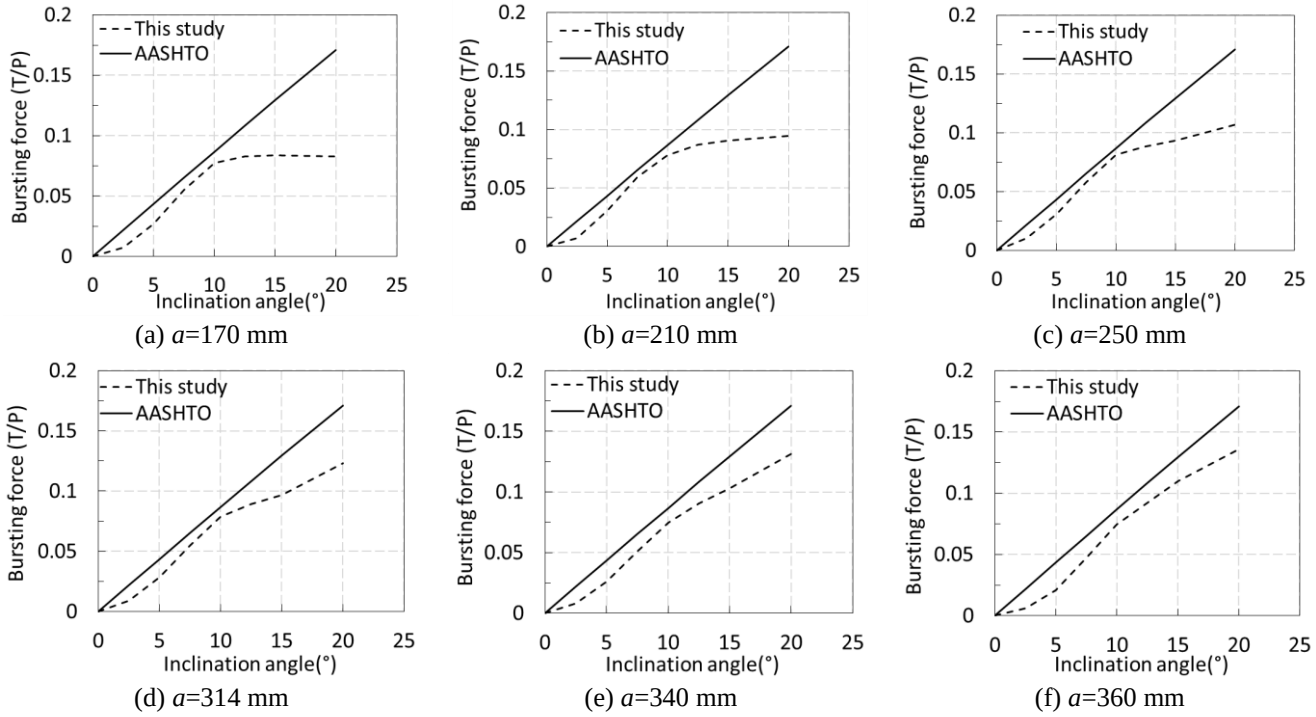

(a) a=170 mm (b) a=210 mm (c) a=250 mm

(d) a=314 mm (e) a=340 mm (f) a=360 mm

Fig. 20 Influence of tendon inclination on the bursting force in the case of b=74 mm

finite element idealization of the anchorage block. When the inclination angle is larger than 10 degree, the duct hole considered in the finite element model pierces the bottom face of the anchorage block (see Fig. 19) while reducing the influencing range subjected to the bursting tensile stress. That is, the bursting tensile stress was distributed to a distance of 1.5h in the length direction when α=0 (see Fig. 11(a)), but this influencing range has been reduced with an increase of the inclination angle when the inclination angle is larger than 10 degrees. Nevertheless, an increase of the bursting tensile stress in proportion to an increase of the inclination angle may counterbalance the decrease of the influencing range and maintain an increase of the bursting force.

In advance, Fig. 20 shows that Eq. (3) is effectively simulates the influence of the inclined tendon and, differently from the previous numerical results obtained for the anchorage blocks without considering a duct hole (Burdet 1990, Songwut 2004, He and Liu 2010), Eq. (3) does not give a conservative result in the anchorage block with a duct hole. This means that Eq. (3) is sufficient to evaluate the bursting force component by the inclined tendon even in the anchorage block with a duct hole. Previous research results conducted without considering the duct hole also show that Eq. (3) can effectively simulate the bursting force component by the inclination of the tendon (Burdet 1990, Jo *et al.* 2002).

4. Equation for bursting force prediction

On the basis of the previous parametric analyses, an improved design equation to evaluate the bursting tensile force in the anchorage block is introduced through the modification of Eq. (1), which has been popularly used in practice. The introduced modification concerns the constant of 0.28 in Eq. (4), which corresponds to 0.25 in the formula introduced in the AASHTO-LRFD design guideline. The use of the constant 0.28 stems from the consideration of the duct hole. The comparisons between T_{burst} obtained from the finite element analyses and T_{burst} evaluated by Eq. (1) mentioned in AASHTO-LRFD and by Eq. (4) introduced in this paper can be found in Figs. 21 and 22. By the use of Eq. (4), as shown in Figs. 21 and 22, improved results relative to those evaluated by Eq. (1) can be expected while reserving the same safety factor in design practice, but the use of Eq. (1) may underestimate the bursting force. In advance, since the basic form and expression of the introduced Eq. (4) are the same as those in Eq. (1), the introduced equation can effectively be used in design practice without any difficulty in application.

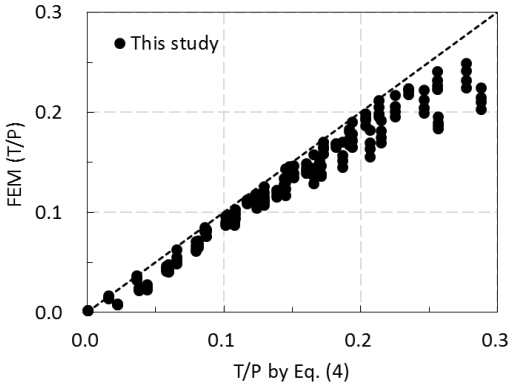

Fig. 21 Comparison between FEM and Eq. (4)

$$T_{burst} = 0.28\Sigma P\left(1-\frac{a}{h}\right) + 0.5|\Sigma(P(\sin\alpha)| \qquad (4)$$

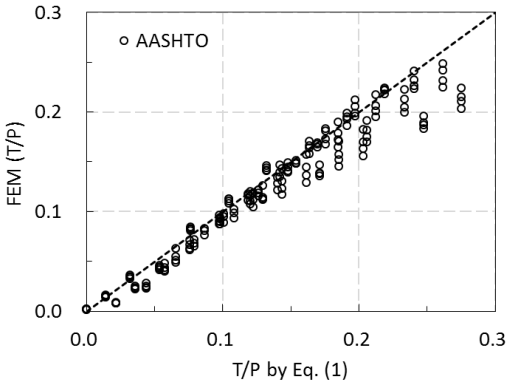

Fig. 22 Comparison between FEM and AASHTO

5. Conclusions

An improved equation to predict the bursting tensile force in the anchorage block is proposed through parametric studies, and no additional understanding is required in using the introduced equation because it maintains the same form and expression as suggested in AASHTO-LRFD. The introduced equation can effectively be used in the preliminary design stage to determine the amount of anchorage reinforcement and to estimate the safety for cracking in the anchorage zone. Nevertheless, an additional verification process through many experimental tests may be required prior to its use as a standard design equation in practice.

Parametric studies to evaluate the influence of many design variables lead to the following conclusions:

(1) Eq. (1) currently used in the design may underestimate the bursting force, which may lead to an unsafe design of the anchorage block.

(2) The influence of the duct hole must be considered in the evaluation of the bursting force.

(3) Since the eccentricity of the anchorage plate decreases the bursting force, its influence on the evaluation of the bursting force can be excluded.

Acknowledgements

This research was supported by a grant (13SCIPA02) from the Smart Civil Infrastructure Research Program funded by the Ministry of Land, Infrastructure and Transport (MOLIT) of the Korean government and the Korea Agency for Infrastructure Technology Advancement(KAIA) and by the Ministry of Land, Infrastructure and Transport (Grant 13IFIP-C113546-01) from the Korea Agency for Infrastructure Technology Advancement(KAIA) grant funded.

References

AASHTO LRFD (2012), AASHTO LRFD Bridge Design Specifications, America Association of State Highway Transportation Officials, Washington, DC, USA

ACI 318 (2014), Building Code Requirements for Structural Concrete and Commentary, American Concrete Instituete, Farmington Hills, MI, USA.

Adeghe, L.N. and Collins, M.P. (1987), "A finite element model for studying reinforced concrete detailing problems", Ph.D. Dissertation, The University of Toronto, Toronto, Canada.

Al-saadoun, S.S. (1980), "A Three-dimensional photoelastic investigation of the stress distribution in the anchorage zone of post- tensioned beams", Master Dissertation, King Fahd University of Petroleum and Minerals, Dhahran, Saudi Arabia.

Breen, J.E., Burdet, O., Roberts, C., Sanders, D. and Wollmann, G. (1994), "Anchorage zone reinforcement for post-tensioned concrete girders", Transportation Research Board, Washington (DC), USA.

Burdet, O. (1990), "Analysis and design of anchorage zones in post-tensioned concrete bridges", Ph.D. Dissertation, The University of Texas, Austin, USA.

CEB-FIP Model Code (2010), Fib Model Code for Concrete Structures, Committee Euro-International du Beton, Lausanne, Switzerland

Choi, K. and Lho, B. (2015), "Study on bursting stress in anchorage zone of prestressed concrete using circular anchorages", *J. Korea Inst. Struct. Mainten. Inspect.*, **19**(1), 3-12.

Choi, K.C., Park, Y.H. and Paik, I.Y. (2010), "Evaluation of bursting behavior in anchorage zone of PSC I girders", *J. Korean Soc. Civil Eng.*, **30**(3), 329-336.

Dassault Systèmes (2013), ABAQUS Online User Manual Version 6.13-1, Dassault Systèmes, Waltham, MA.

denColln Uijl, J.A. (1983), "Tensile stresses in the transmission zones of hollow-core slabs prestressed with pretensioned strands", Delft University of Technology, Stevin Laboratory, Delft, Netherlands.

Douglas, D.J. and Trahair, N.S. (1960), "An examination of the stresses in the anchorage zone of a post-tensioned prestressed concrete beam", *Mag. Concrete Res.*, **12**(34), 9-18.

Fenwick, R.C. and Lee, S.C. (1986), "Anchorage zones in prestressed concrete members", *Mag. Concrete Res.*, **38**(135), 77-89.

Haroon, S., Yazdani, N. and Tawfiq, K. (2006), "Posttensioned anchorage zone enhancement with fiber-reinforced concrete", *J. Bridge Eng.*, **11**(5), 566-572.

He, Z. and Liu, Z. (2011), "Investigation of bursting forces in anchorage zones: compression-dispersion models and unified design equation", *J. Bridge Eng.*, **16**(6), 820-827.

Hou, D.W., Zhao, J.L., Shen, J.S.L. and Chen, J. (2017), "Investigation and improvement of strut-and-tie model for design of end anchorage zone in post-tensioned concrete structure", *Constr. Build. Mater.*, **136**, 482-494.

Jo, B., Byun, Y. and Tae, G. (2002), "Structural behavior of cable anchorage zones in prestressed concrete cable-stayed bridge", *Can. J. Civil Eng.*, **29**(1), 171-180.

Kara, M.E., Firat, F.K., Sonmez, M. and Karabork, T. (2016), "An investigation of anchorage to the edge of steel plates bonded to RC structures", *Steel Compos. Struct.*, **22**(1), 25-43.

Kim, J., Yang, J. and Kwon, Y. (2016), "Influence of steel fiber and reinforcing details on the ultimate bearing strength of the post-tensioning anchorage zone", *Struct. Eng. Mech.*, **59**(5), 867-883.

Kim, J.K., Kwon, Y. and Kwak, H.G. (2014), "Anchorage zone behavior in the slab with flat anchorage", *J. Korean Soc. Hazard Mitigat.*, **14**(1), 67-76.

Kim, J.K., Yang, J.M. and Yim, H.J. (2016), "Experimental evaluation of transfer length in pretensioned concrete beams using 2,400-MPa prestressed strands", *J. Struct. Eng.*, **142**(11), 4016088.

Liu, C., Xu, D., Jung, B. and Morgenthal, G. (2013), "Reinforcement design for the anchorage of externally

prestressed bridges with "tensile stress region", *Comput. Concrete*, **11**(5), 383-397.
O'Callaghan, M.R. and Bayrak, O. (2008), "Tensile stresses in the end regions of pretensioned I-beams at release", Master Dissertation, The University of Texas, Austin, USA.
Oh, B.H. and Lim, D.H. (1995), "Stress distribution and crack control at anchorage zones in prestressed concrete box-girder bridge members", *J. Korean Soc. Civil Eng.*, **15**(2), 325-336.
Oh, B.H., Lim, D.H. and Park, S.S. (1997), "Stress distribution and cracking behavior at anchorage zones in prestressed concrete members", *ACI Struct. J.*, **94**(5), 549-557.
Okumus, P., Oliva, M.G. and Becker, S. (2012), "Nonlinear finite element modeling of cracking at ends of pretensioned bridge girders", *Eng. Struct.*, **40**, 267-275.
Robinson, B., Florida, A., Tawfiq, K.S. and Engineering, F.C. (2009), "Using steel fiber reinforced concrete in post-tensioned anchorage zones", *Structures Congress 2009: Don't Mess with Structural Engineers: Expanding Our Role*, Austin, Texas, USA, May.
Sahoo, D.K., Singh, B. and Bhargava, P. (2009), "Investigation of dispersion of compression in bottle-shaped struts", *ACI Struct. J.*, **106**(2), 178-186.
Sanders, D.H. and Breen, J.E. (1997), "Post-tensioned anchorage zones with single straight concentric Anchorages", *ACI Struct. J.*, **94**(2), 146-158.
Schlaich, J., Schäfer, K. and Jennewein, M. (1987), "Toward a consistent design of structural concrete", *PCI J.*, **32**(3), 74-150.
Shen, S.L., Hou, D.W., Zhao, J.L., Horpibulsuk, S. and Yin, Z.Y. (2014), "Assessment of internal forces for intermediate anchorage zone of post-tensioned concrete structure", *Constr. Build. Mater.*, **64**, 370-378.
Songwut, H. (2004), "Linear and nonlinear finite element analyses of anchorage zones in post-tensioned concrete structures", Ph.D. Dissertation, Virginia Polytechnic Institute and State University, Blacksburg, USA.
Stone, W.C. and Breen, J.E. (1984), "Behavior of post-tensioned girder anchorage zones", *PCI J.*, **29**(1), 64-109.
Sundara Raja Iyengar, K.T. and Yogananda, C.V. (1966), "A three-dimensional stress distribution problem in the anchorage zone of a post-tensioned concrete beam", *Mag. Concrete Res.*, **18**(55), 75-84.
Wollmann, G.P. (1992), "Anchorage zones in post-tensioned concrete structure", Ph.D. Dissertation, The University of Texas, Austin, USA.
Wollmann, G.P., Breen, J.E. and Kreger, M.E. (2000), "Anchorage of external tendons in end diaphragms", *J. Bridge Eng.*, **5**(3), 208-215.
Yettram, A.L. and Robbins, K. (1970), "Anchorage zone stresses in post-tensioned uniform members with eccentric and multiple anchorages", *Mag. Concrete Res.*, **22**(73), 209-218.
Yun, Y.M. (2005), "Evaluation of ultimate strength of post-tensioned anchorage zones", *J. Adv. Concrete Technol.*, **3**(1), 149-159.
Zhao, J.L., Shen, S.L., Wang, L.B. and Chen, J. (2011), "A design approach for the interior anchorage zone of post-tensioned concrete structure", *KSCE J. Civil Eng.*, **15**(3), 487-495.
Zhou, L. and Liu, Z. (2016), "Transverse bursting stresses due to horizontally curved tendons in the top slab of box girders", *J. Bridge Eng.*, **21**(2), 1-10.
Zhou, L.Y., Liu, Z. and He, Z.Q. (2015), "Further investigation of transverse stresses and bursting forces in post-tensioned anchorage zones", *Struct. Concrete*, **16**(1), 84-92.